Polymer xxx (2015) 1–9

Contents lists available at ScienceDirect

Polymer

journal homepage: www.elsevier.com/locate/polymer

Self-healing response in supramolecular polymers based on reversible zinc–histidine interactions

Marcel Enke [a, b], Stefan Bode [a, b], Jürgen Vitz [a, b], Felix H. Schacher [a, b], Matthew J. Harrington [c], Martin D. Hager [a, b, *, 1], Ulrich S. Schubert [a, b, *, 1]

[a] Laboratory of Organic and Macromolecular Chemistry (IOMC), Friedrich Schiller University Jena, Humboldtstr. 10, 07743 Jena, Germany
[b] Jena Center for Soft Matter (JCSM), Friedrich Schiller University Jena, Philosophenweg 7, 07743 Jena, Germany
[c] Department of Biomaterials, Max Planck Institute for Colloids and Interfaces, Potsdam 14424, Germany

ARTICLE INFO

Article history:
Received 29 December 2014
Received in revised form
21 March 2015
Accepted 24 March 2015
Available online xxx

Keywords:
Self-healing polymers
Bio-inspired materials
Metallopolymers

ABSTRACT

Histidine-metal interactions are utilized in many biological materials as reinforcing crosslinks, and in particular, are believed to contribute as reversible crosslinks to the intrinsic self-recovery behavior of mussel byssal threads. In this contribution, two new histidine-based monomers were synthesized and further copolymerized with butyl methacrylate (BMA) and lauryl methacrylate (LMA) applying the reversible addition–fragmentation chain transfer (RAFT) polymerization technique. Crosslinking with zinc ions resulted in supramolecular metallopolymer networks exhibiting a self-healing behavior that was tunable depending on the specific zinc salt used. The presented results provide a class of new polymeric species with different self-healing capacities.

1. Introduction

Since the pioneering work of Dry et al. [1] and White et al. [2] numerous strategies for the design of self-healing polymers have been investigated and developed. Currently, there is a strong interest and potential for developing new strategies for promising and robust self-healing polymers inspired by natural materials, *e.g.*, based on the self-renewal of *Hydra* [3], the recovery of egg capsules of marine whelks [4], or the self-healing behavior of mussel byssal threads [5]. The basic mechanism for the design of self-healing materials can be divided into two classes: Extrinsic and intrinsic. Extrinsic self-healing materials are based on external healing compounds, which are primarily encapsulated within the polymer matrix. After damage, the mobile phase (*i.e.* the healing agent) fills the crack and after subsequent polymerization with the help of a catalyst, the original mechanical properties can be regenerated [2]. In contrast, intrinsic self-healing polymers are based on specific reversible chemical bonds or physical interactions, which enable repetitive healing cycles of the materials [6,7]. Suitable approaches for introducing self-healing properties into polymeric materials are the utilization of Diels Alder reactions [8–11], disulfide bridges [12–14], hydrogen bonds [15–18], π-π interactions [19–22], ionic interactions [23,24], or metal-ligand interactions [25–30].

Metal-ligand interactions are also found in a number of natural systems, where they contribute to materials properties such as adhesion, toughness, hardening and, most importantly, for the current study, self-healing [5]. A prominent example of a self-healing natural material that is mediated by metal complexation is the mussel byssus, which contains both 3,4-dihydroxy-phenylalanine (DOPA) coordinated to iron ions [31,32], as well as histidine metal interactions [33,34]. The byssus is comprised of a bundle of fiber-like threads, which fasten the organism to rocks in seashore habitats and dissipate energy during cyclic loading by waves. Notably, the distal region of the byssal thread exhibits intrinsic self-healing of the mechanical stiffness following damage when loaded beyond the yield point [35]. Several studies suggest that histidine–zinc coordination interactions in the primary protein components, the preCols, are responsible for this behavior which is proposed to occur via reversible rupture and reformation of the histidine–zinc complexes. [5, 34, 36, 37]

Previously, PEG-based hydrogels with histidine side chains [38] and histidine-rich peptides [37] have demonstrated the potential for applying the lessons of the mussel byssus to synthetic materials. Another study reinforces polymers based on imidazole-metal

* Corresponding authors. Laboratory of Organic and Macromolecular Chemistry (IOMC), Friedrich Schiller University Jena, Humboldtstr. 10, 07743 Jena, Germany.
E-mail addresses: martin.hager@uni-jena.de (M.D. Hager), ulrich.schubert@uni-jena.de (U.S. Schubert).
[1] www.schubert-group.de.

http://dx.doi.org/10.1016/j.polymer.2015.03.068
0032-3861/

interactions [39]. Furthermore, zinc–imidazole interactions in acrylate based brush copolymers revealed excellent self-healing properties, which were investigated by tensile mechanical tests [30]. The present study provides, to the best of our knowledge, the first example utilizing the zinc–histidine interactions to produce self-healing coatings. In the present study, histidine-containing copolymers were synthesized via reversible addition–fragmentation chain transfer (RAFT) polymerization and further crosslinked with different zinc salts. These model systems were investigated with respect to their self-healing ability and, notably, revealed that self-healing properties are tunable based on the specific zinc salt chosen to crosslink.

2. Experimental section

2.1. Materials and instrumentation

All chemicals used were purchased from Fluka, Aldrich, TCI, VWR, Alfa Aesar and ABCR. They were used without further purification. Butyl methacrylate and lauryl methacrylate were passed over a short neutral aluminum oxide plug. The solvents were dried with activated mol sieves (DMF) and calcium chloride (dichloromethane, chloroform, triethylamine). Chromatographic separation was performed with silica gel 60 from Merck. The reaction progress was monitored by thin layer chromatography (TLC) using aluminum sheets precoated with silica gel 60 F_{254} (Merck). 1D (^{1}H, ^{13}C) nuclear magnetic resonance spectra were recorded on a Bruker AC 400 (400 MHz), a Bruker AC 300 (300 MHz) and a Bruker AC 250 (250 MHz) at 298 K. Chemical shifts are reported in parts per million (ppm, δ scale) relative to the residual signal of the solvent. Coupling constants are given in Hz. Polymeric samples were measured with an extended number of scans (min. 512) and an extended relaxation time ($t_1 = 10$ s). ESI-Q-TOF MS measurements were performed using a micrOTOF (Bruker Daltonics) mass spectrometer equipped with an automatic syringe pump, which is supplied from KD Scientific for sample injection. The mass spectrometer was operating in the positive ion mode. The standard electrospray ion (ESI) source was used to generate the ions. Samples' concentrations ranging from 1 to 10 μg/mL were injected using a constant flow (3 μL/min) of sample solution. ESI solvents used in this study were dichloromethane, acetonitrile, chloroform or their mixtures. The ESI-Q-TOF MS instrument was calibrated in the *m/z* range 50 to 3000 using an internal calibration standard (Tunemix solution) from Agilent. Data and HR-MS calculations were processed via the Bruker Data Analysis software version 4.0. Elemental analyses were carried out on a Vario El III (Elementar) elemental analyzer. Size exclusion chromatography (SEC) measurements were performed on two different set-ups: a) Shimadzu with SCL-10A VP (system controller), LC-10AD VP (pump), SIL-10AD VP (auto sampler), CTO-10A VP (oven), RID-10A (RI detector), PSS SDV guard/lin S (5 μm particle size) (column), chloroform/*iso*-propanol/trieethylamine [94/2/4] (eluent), 1 mL/min at RT (flow rate and temperature) and poly(methyl methacrylate) (standard). b) Shimadzu with SCL-10A VP (system controller), DGU-14A (degasser), LC-10AD VP (pump), SIL-10AD VP (auto sampler), RID-10A (RI detector), PSS GRAM guard/1000/30 Å (column), DMAc + 0.21% LiCl (eluent), 1 mL/min at 40 °C (flow rate and temperature) and poly(methyl methacrylate) (standard). The TGA analysis was carried out under helium using an STA Netzsch 449 F3 Jupiter and the DSC investigations was performed on a DSC 204 F1 Phoenix by Netzsch under a nitrogen atmosphere with a heating rate of 10 or 20 K/min. The UV-Vis spectra were measured with a PerkinElmer Lambda 45 UV/VIS spectrometer. Small angle X-ray scattering (SAXS) measurements were performed on a Bruker AXS Nanostar (Bruker, Karlsruhe, Germany), equipped with a microfocus X-ray source (Incoatec $I\mu S_{Cu}$ E025, Incoatec, Geesthacht, Germany), operated at $\lambda = 1.54$ Å. A pinhole setup with 750 μm, 400 μm, and 1000 μm (in the order from source to sample) was used and the sample-to-detector distance was 107 cm. Samples were mounted on a metal rack and fixed using tape. The scattering patterns were corrected for the beam stop and the background (Scotch tape) prior to evaluations. Temperature ramps were performed from 20 to 120 °C in $\Delta T = 20$ K. The measurement time was always 3 h. The self-healing behavior was studied with the help of an optical microscope by cutting the copolymer films resulting in scratches on the micrometer scale and afterwards heating to a defined temperature. The self-healing behavior of the polymers was tested at 100 °C. If a healing was obtained, the temperature was reduced until no self-healing behavior could be monitored. If the polymer did not heal at 100 °C, the temperature was increased,. The maximum temperature was 150 °C. The elastic moduli of the materials were characterized via depth-sensing indentation (DSI) using a TriboIndenter TI 900 (Hysitron Inc., Minneapolis, MN) with a NanoDMA 06 transducer, equipped with a conospherical diamond indenter tip of ~4.7 μm radius. The polymer was directly synthesized on a glass cavity slide. Afterwards, the polymer film was dried for 1 week at ambient temperature and humidity. The depth-sensing indentation (DSI) was conducted at ambient conditions at 23.8 ± 0.1 °C and 18.0 ± 2.5% relative humidity (RH). For quasi-static testing, a 1 s loading, 2 s hold at maximum load, and 1 s unloading profile was applied.[40–42] All measurements were performed in a single automated run in less than 3 h for each sample. The reduced modulus E_r was determined from the unloading response utilizing the analysis method proposed by Oliver and Pharr. [43,44] Measurements were repeated at sixteen maximum loads, increasing in steps of 140 μN from 100 μN to 2200 μN and from 2000 μN to 4100 μN. The values were averaged, measurements outside the area function limits were excluded. From the reduced modulus E_r, the indentation modulus E_i was calculated using the elastic modulus and Poisson's ratio of the diamond indenter, 1140 GPa and 0.07, respectively, and a Poisson's ratio of 0.4 for the polymeric material, according to

$$E_{i,sample} = \frac{1 - \nu^2_{sample}}{\frac{1}{E_{r,sample}} - \frac{1-\nu^2_{indenter}}{E_{indenter}}}$$

The hardness has the normal definition:

$$H = \frac{P_{max}}{A}$$

2.2. Synthesis of histidine monomers

N^{τ}-Tritylhistidine methyl ester (**1**) and N^{τ}-tritylhistidine (**2**) were prepared according to literature. The detailed procedures are described in the SI [45,46].

2.2.1. N^{α}-Methacryloyl-N^{τ}-tritylhistidine methyl ester (**3**)

1 (2.00 g, 4.86 mmol) was dissolved in 50 mL dry dichloromethane under nitrogen atmosphere. Triethylamine (1.36 mL, 9.74 mmol) was added and after 15 min methacrylic anhydride (0.73 mL, 4.86 mmol) was added dropwise. After complete conversion, which was monitored by TLC, the solvent and the triethylamine were evaporated in *vacuo*. The residue was dissolved in 50 mL chloroform and washed three times with 50 mL deionized water. The organic layer was dried over Na_2SO_4. Subsequently, the crude product was purified by silica gel chromatography (MeOH/$CHCl_3$ 1:20, $R_f = 0.45$).

Yield: 1.9 g of a light yellow solid, 82%.

Melting point: 47 − 48 °C.

Please cite this article in press as: Enke M, et al., Self-healing response in supramolecular polymers based on reversible zinc–histidine interactions, Polymer (2015), http://dx.doi.org/10.1016/j.polymer.2015.03.068

^{1}H NMR (300 MHz, $CDCl_3$): δ = 1.97 (s, 3H, $-CH_3$), 3.06 (dq, J = 4.8 Hz, 12.6 Hz, 2H, $-CH_2-$), 3.61 (s, 3H, $-OCH_3$), 4.82 (m, 1H, $-CH-$), 5.34 (s, 1H, $=CH_2$), 5.81 (s, 1H, $=CH_2$), 6.55 (s, 1H, $H-^2$Im), 7.08 – 7.13 (m, 6H, *H*-aromatic), 7.31 – 7.34 (m, 9H, *H*-aromatic), 7.37 (s, 1H, $H-^5$Im), 7.80 (d, J = 7.6 Hz, 1H, $-NH-$) ppm.

^{13}C NMR (75 MHz, $CDCl_3$): δ = 18.6 ($-CH_3$), 29.8 ($-CH_2-$), 52.2 ($-OCH_3$), 52.8 ($-CH-$), 75.4 ($-C-Ph^3$), 119.8 ($=CH_2$), 120.4 ($C-^2$Im), 128.2 ($C-^4$Ph; $C-^2$Ph; $C-^6$Ph), 129.9 ($C-^3$Ph; $C-^5$Ph), 136.8 ($C-^3$Im), 138.9 ($C-^5$Im), 139.6 ($C-^1$Ph), 142.4 ($C=CH_2$), 168,1 ($-NH-C=O$), 172.0 ($C=O$) ppm.

ESI-TOF MS (HR MS): calc.: m/z = 480.2282 $[M+H]^+$; found: m/z = 480.2263 $[M+H]^+$; error: 3.9 ppm.

2.2.2. N^{α}-Methacryloyl-N^{τ}-tritylhistidine (**4**)

2 (1.50 g, 3.77 mmol) was dissolved in 50 mL dry dichloromethane under nitrogen atmosphere. Subsequently, triethylamine (1.05 mL, 7.45 mmol) and DMAP (10 mol%) were added. After 15 min, methacrylic anhydride (0.56 mL, 3.77 mmol) was added dropwise. After complete conversion, which was monitored by TLC, the solvent and the triethylamine were evaporated in *vacuo* and the residue was dissolved in 50 mL chloroform. The organic layer was washed three times with deionized water and dried over Na_2SO_4. Purification by silica gel chromatography (MeOH/$CHCl_3$ 1:10, R_f = 0.4) leads to the product.

Yield: 1.25 g of a white solid, 71%.

Melting point: 124 – 125 °C.

^{1}H NMR (300 MHz, $CDCl_3$): δ = 1.82 (s, 3H, $-CH_3$), 3.22 (s, 2H, $-CH_2-$), 4.52 (s, 1H, $-CH-$), 5.21 (s, 1H, $=CH_2$), 5.53 (s, 1H, $=CH_2$), 6.57 (s, 1H, $H-^2$Im), 6.92 – 7.41 (m, 15H, *H*-aromatic), 7.68 (s, 1H, $H-^5$Im), 10.11 (bs, 1H, $-OH$) ppm.

^{13}C NMR (75 MHz, $CDCl_3$): δ = 18.7 ($-CH_3$), 28.8 ($-CH_2-$), 54.1 ($-CH-$), 75.8($-C-Ph^3$), 119.7 ($=CH_2$), 120.4 ($C-^2$Im), 128.3 ($C-^4$Ph), 128.9 ($C-^2$Ph; $C-^6$Ph), 129.8 ($C-^3$Ph; $C-^5$Ph), 139.9 ($C-^3$Im), 140.7 ($C-^5$Im), 142.0 ($C-^1$Ph), 144.1 ($C=CH_2$), 167,7 ($-NH-C=O$), 177.4 ($C=O$) ppm.

ESI-TOF MS (HR MS): calc.: m/z = 466.2125 $[M+H]^+$; found: m/z = 466.2105 $[M+H]^+$; error: 4.3 ppm.

2.3. Synthesis of histidine containing copolymers

2.3.1. RAFT polymerization of ***P1*** to ***P4***

In a 20 mL microwave vial the desired amounts of the two monomers were dissolved in dry DMF. Afterwards, the exact volumes of the stock solutions of the RAFT agent (CTA) and AIBN in DMF were added. The [M] to [CTA] ratio was always 150/1 and the ratio of [CTA] to [AIBN] 4/1. The ratio between BMA/LMA and histidine monomer was held constant at 10:1. The reaction mixture was degassed with nitrogen for 30 min. The reaction was performed at 70 °C overnight. All reaction details are summarized in Table 1. Subsequently, the resulting polymers were precipitated twice in ice-cold methanol.

P1

^{1}H NMR (300 MHz, $CDCl_3$): δ = 0.78 – 2.17 (132H), 2.79 – 3.10 (2H), 3.45 – 3.65 (3H), 3.84 – 4.10 (11H), 4.65 (1H), 6.57 (1H), 7.04 – 7.47 (16H), 7.84 – 8.10 (1H) ppm.

SEC (DMAc + 0.21% LiCl): M_n = 15,500 g/mol; M_w = 16,800 g/mol; PDI = 1.08.

EA: found: C: 69.30%; H: 9.26%; N: 1.70%.

DSC: T_g: 45 °C; **TGA:** T_d: 288 °C.

P2

^{1}H NMR (300 MHz, $CDCl_3$): δ = 0.58 – 2.13 (230H), 2.80 – 3.08 (2H), 3.43 – 3.61 (3H), 3.79 – 4.06 (10H), 4.62 (1H), 6.56 (1H), 7.05 – 7.38 (16H), 7.87 (1H) ppm.

SEC ($CHCl_3$/IPA/TEA): M_n = 29,900 g/mol; M_w = 34,800 g/mol; PDI = 1.16.

EA: found: C: 75.52%; H: 11.20%; N: 1.18%.

DSC: no T_g observed; **TGA:** T_d: 307 °C.

P3

^{1}H NMR (300 MHz, $CDCl_3$): δ = 0.57 – 2.02 (120H), 2.65 – 2.85 (1H), 3.10 – 3.27 (1H), 3.77 – 4.06 (10H), 4.33 (1H), 6.54 – 7.70 (17H) ppm.

SEC (DMAc + 0.21% LiCl): M_n = 14,800 g/mol; M_w = 17,400 g/mol; PDI = 1.17.

EA: found: C: 66.81%; H: 8.63%; N: 2.26%.

DSC: T_g: 50 °C; **TGA:** T_d: 312 °C.

P4

^{1}H NMR (300 MHz, $CDCl_3$): δ = 0.75 – 2.04 (345H), 2.85 (1H), 3.25 (1H), 3.84 – 4.06 (15H), 4.14 (1H), 7.15 – 7.56 (17H) ppm.

SEC ($CHCl_3$/IPA/TEA): M_n = 22,400 g/mol; M_w = 34,200 g/mol; PDI = 1.53.

EA: found: C: 75.35%; H: 11.55%; N: 0.63%.

DSC: no T_g observed; **TGA:** T_d: 230 °C.

2.3.2. Cleavage of the trityl-group of histidine containing polymers (***P5*** to ***P8***)

In a 100 mL one neck flask the desired amount of polymer was dissolved in 30 mL chloroform. Afterwards the same volume of trifluoroacetic acid (TFA) was added. Additionally, triethylsilane was added as scavenger and the solution was stirred for 2 h at room temperature. The reaction mixture was washed with 50 mL water and 50 mL aqueous saturated $NaHCO_3$ solution. The organic layer was dried over Na_2SO_4 and concentrated. The resulting viscous solution was precipitated in cold methanol. All reaction details are summarized in Table 2.

P5

^{1}H NMR (300 MHz, $CDCl_3$): δ = 0.87 – 1.90 (120H), 3.12 (2H), 3.68 (3H), 3.85 – 4.12 (10H), 4.65 (1H), 6.84 (1H), 7.80 (1H) ppm.

SEC (DMAc + LiCl): M_n = 18,000 g/mol; M_w = 19,500 g/mol; PDI = 1.08.

EA: found: C: 66.89%; H: 9.51%; N: 1.67%.

DSC: T_g: 38 °C; **TGA:** T_d: 346 °C.

P6

^{1}H NMR (300 MHz, $CDCl_3$): δ = 0.86 – 1.89 (253H), 3.17 (2H), 3.70 (3H), 3.85 – 4.05 (11H), 4.61 (1H), 6.91 (1H), 7.73 (1H), 7.87 (1H) ppm.

SEC ($CHCl_3$/IPA/TEA): M_n = 31,800 g/mol; M_w = 35,100 g/mol; PDI = 1.10.

EA: found: C: 74.42%; H: 11.50%; N: 1.16%.

DSC: T_g: 45 °C; **TGA:** T_d: 241 °C.

P7

^{1}H NMR (300 MHz, $CDCl_3$): δ = 0.57 – 1.89 (132H), 2.92 (2H), 3.73 – 4.15 (11H), 4.45 (1H), 6.95 (1H), 7.61 (1H) ppm.

SEC (DMAc + LiCl): M_n = 16,600 g/mol; M_w = 19,400 g/mol; PDI = 1.16.

EA: found: C: 65.22%; H: 9.32%; N: 2.27%.

DSC: no T_g observed; **TGA:** T_d: 302 °C.

P8

^{1}H NMR (300 MHz, $CDCl_3$): δ = 0.85 – 1.90 (345H), 2.94 (2H), 3.76 – 4.14 (15H), 4.49 (1H), 6.86 (1H), 7.68 (1H) ppm.

SEC ($CHCl_3$/IPA/TEA): M_n = 22,100 g/mol; M_w = 29,300 g/mol; PDI = 1.33.

EA: found: C: 75.12%; H: 11.73%; N: 0.52%.

DSC: no T_g observed; **TGA:** T_d: 218 °C.

2.3.3. General procedure for the crosslinking of the polymers (***MP1*** to ***MP24***)

In a 5 mL vial the desired amount of polymer was dissolved in 1 mL chloroform. A solution of the metal salt in 1 mL methanol was added. The ratio between the histidine unit of the polymers and the metal salt was always 3:1. The used amounts of polymer and of the

Please cite this article in press as: Enke M, et al., Self-healing response in supramolecular polymers based on reversible zinc–histidine interactions, Polymer (2015), http://dx.doi.org/10.1016/j.polymer.2015.03.068

Table 1
Overview of the reaction details of the RAFT polymerizations (**P1** to **P4**).

Sample	Monomers	m (monomers) [g]	m (AIBN) [mg]	m (CTA) [mg]	V (solvent) [mL]	Reaction time [h]
P1	**3**	0.51	3.18	CPDB	DMF	19
	BMA	1.50		17.12	5.80	
P2	**3**	0.28	1.77	CPDB	DMF	19
	LMA	1.50		9.57	3.24	
P3	**4**	1.03	3.49	CDP	DMF	24
	BMA	1.50		34.35	6.38	
P4	**4**	0.77	2.60	CDP	DMF	24
	LMA	2.00		25.60	4.76	

metal salts are listed in Table 3. Afterwards the solvents were slowly evaporated. The resulting metallopolymers were washed with 1 mL methanol to remove uncomplexed salt and were dried in *vacuo*. The results of elemental analysis and the thermal properties are summarized in Table S1.

3. Results and discussion

In order to synthesize the metallopolymers, two new histidine-containing monomers were firstly prepared: N^{α}-Methacryloyl-N^{τ}-tritylhistidine methyl ester (**3**) and N^{α}-methacryloyl-N^{τ}-tritylhistidine (**4**). The first monomer bears a methyl ester function and the second one a free carboxylic acid function, which may result in different self-healing abilities of the resulting metallopolymers. The presence of free carboxylic acid in monomer **4** may also be relevant in the mechanical behavior of the byssus, considering the elevated concentration of aspartate and isoasparate residues in the mature thread matrix protein, TMP-1 [47], and the known tendency of the carboxylate group of aspartic acid to coordinate zinc ions [48].

In the first step of the monomer synthesis, a triphenyl methyl (Trt-) group was introduced to protect the ^{1}Im-amine in order to improve the solubility and the purification procedure of the histidine derivates. Due to this improvement of the synthetic pathway, the product could be obtained by the reaction with methacrylic anhydride in high yields (Scheme 1). The purity of both monomers could be proven by ^{1}H NMR spectroscopy and ESI-MS measurements (Fig. S1 and Fig. S2).

Afterwards, the histidine monomers were copolymerized with butyl methacrylate (BMA) and lauryl methacrylate (LMA) using the reversible addition–fragmentation chain transfer (RAFT) polymerization technique to obtain well-defined polymers with low PDI values (for most polymers < 1.2) [49–51]. Copolymers containing **3** were prepared with AIBN and 2-cyanopropan-2-yl benzodithioate (CPDB). In contrast, monomer **4** did not copolymerize with BMA/LMA by the utilization of CPDB. Thus, 4-cyano-4-[(dodecylsulfanylthiocarbonyl)sulfanyl] pentanoic acid (CDP) was used to synthesize **P3** and **P4**. The desired content of histidine of about 10% could be achieved, except for **P4** (Table 4). The histidine contents were determined by ^{1}H NMR spectroscopy. In addition, the amount of histidine was calculated from the results of the elemental analysis (percent value of nitrogen). The resulting concentrations are comparable for most of the copolymers; however, these values were slightly lower than those determined by ^{1}H NMR spectroscopy. Due to the low nitrogen content (~2%), the elemental analysis instrument error could have a large influence on the accurate determination of the histidine content, therefore, the copolymer composition was determined by ^{1}H NMR spectroscopy, which provides more accurate results. These were utilized for further calculations. After the synthesis of the histidine containing copolymers, the protecting group was removed in order to mimic the mussel system [52]. The complete cleavage of the protecting group could be proven by ^{1}H NMR (Fig. S3) and UV/Vis spectroscopy (Fig. 1). The Trt-protection unit has a prominent absorption maximum at 250 nm. **P1** shows this absorption maximum as well as a local maximum at 302 nm resulting from the RAFT-endgroup [53]. After the cleavage of the Trt-group, the Trt-signal vanished and the RAFT-endgroup signal dominates the resulting absorption spectrum of **P5**.

Table 2
Overview of the reaction details of the post-polymerization cleavage of the trityl-group (**P4** to **P8**).

Sample	Used polymers	m (polymers) [g]	V (Et_3SiH) [μL]
P5	**P1**	0.80	18
P6	**P2**	1.18	30
P7	**P3**	1.05	30
P8	**P4**	1.17	30

During the cleavage of the Trt-group with trifluoroacetic acid a small amount of histidine was removed as well, which is due to the instability of amides against acids (Table 4). The SEC results and the thermal properties of the resulting copolymers are summarized in Table 4. Unexpectedly, after cleavage of the Trt-group, the molar masses of the polymers are higher than before; however, this may be explained by a different hydrodynamic behavior of the polymer chains due to the possibility to form hydrogen bonds. The glass transition temperatures (T_g) of the copolymers are in the range of 38 − 50 °C (Fig. S5). The LMA-containing polymers showed no T_g, however, endothermic peaks could be obtained at approximately −35 °C (Fig. S6). These peaks indicate side-chain crystallization of the poly(lauryl methacrylate) (PLMA) chains [54]. All copolymers are thermally stable up to at least ~230 °C.

In order to investigate the self-healing abilities, the copolymers **P1** to **P8** were crosslinked by the addition of zinc(II) chloride, zinc(II) acetate and zinc(II) nitrate in the ratio for Zn:His of 1:3 (Scheme 2). While the detailed coordination geometry of zinc and histidine is still unknown in the mussel byssus, X-ray absorption spectroscopy of jaws of the marine worm *Nereis* sp. suggests the presence of His_3-Zn complexes [55].

The resulting metallopolymer networks (**MP1** to **MP24**) were analyzed by differential scanning calorimetry (DSC) and thermogravimetric analysis (TGA). The summary of the thermal properties is listed in Table S1. In general, the T_g values of the BMA-containing metallopolymers are higher than those with a PLMA-backbone (ca. 70 K). Due to the longer side chains of PLMA compared to PBMA the copolymer backbone is more flexible, which likely results in a lower T_g (ca. −50 °C) [56]. In addition, the metallopolymers are stable up to 190 °C. TGA measurements also indicated that at 800 °C approximately 2 − 5% of material is remaining (*e.g.*, zinc containing compounds). Thus, the exact coordination structure cannot be calculated from these data [26]. Furthermore, the networks were analyzed by small angle X-ray scattering (SAXS). In contrast to the previously described metallopolymers with terpyridine metal interactions [25,26], the measurements revealed no significant reflexes (Fig. S7). As a result, the weaker zinc–histidine interactions compared with relatively strong iron/cadmium terpyridine

Please cite this article in press as: Enke M, et al., Self-healing response in supramolecular polymers based on reversible zinc–histidine interactions, Polymer (2015), http://dx.doi.org/10.1016/j.polymer.2015.03.068

Table 3
Overview of the reaction details of the crosslinking reactions (**MP1** to **MP24**).

Metallopolymer	Used polymer	Amount of the polymer [mg]	Used metal salt	Amount of the metal salt [mg]
MP1	**P1**	48.3	$ZnCl_2$	1.1
MP2	**P1**	49.5	$Zn(OAc)_2 \times 2H_2O$	1.8
MP3	**P1**	48.9	$Zn(NO_3)_2 \times 6H_2O$	2.4
MP4	**P2**	54.5	$ZnCl_2$	0.8
MP5	**P2**	56.0	$Zn(OAc)_2 \times 2H_2O$	1.3
MP6	**P2**	48.8	$Zn(NO_3)_2 \times 6H_2O$	1.7
MP7	**P3**	50.4	$ZnCl_2$	1.2
MP8	**P3**	52.6	$Zn(OAc)_2 \times 2H_2O$	2.0
MP9	**P3**	50.6	$Zn(NO_3)_2 \times 6H_2O$	2.7
MP10	**P4**	56.9	$ZnCl_2$	0.6
MP11	**P4**	51.3	$Zn(OAc)_2 \times 2H_2O$	0.9
MP12	**P4**	55.4	$Zn(NO_3)_2 \times 6H_2O$	1.3
MP13	**P5**	48.8	$ZnCl_2$	1.2
MP14	**P5**	52.8	$Zn(OAc)_2 \times 2H_2O$	2.1
MP15	**P5**	49.2	$Zn(NO_3)_2 \times 6H_2O$	2.7
MP16	**P6**	52.7	$ZnCl_2$	0.9
MP17	**P6**	49.5	$Zn(OAc)_2 \times 2H_2O$	1.3
MP18	**P6**	56.4	$Zn(NO_3)_2 \times 6H_2O$	2.0
MP19	**P7**	49.8	$ZnCl_2$	1.4
MP20	**P7**	51.7	$Zn(OAc)_2 \times 2H_2O$	2.3
MP21	**P7**	50.7	$Zn(NO_3)_2 \times 6H_2O$	2.9
MP22	**P8**	55.8	$ZnCl_2$	0.6
MP23	**P8**	53.9	$Zn(OAc)_2 \times 2H_2O$	1.0
MP24	**P8**	51.8	$Zn(NO_3)_2 \times 6H_2O$	1.2

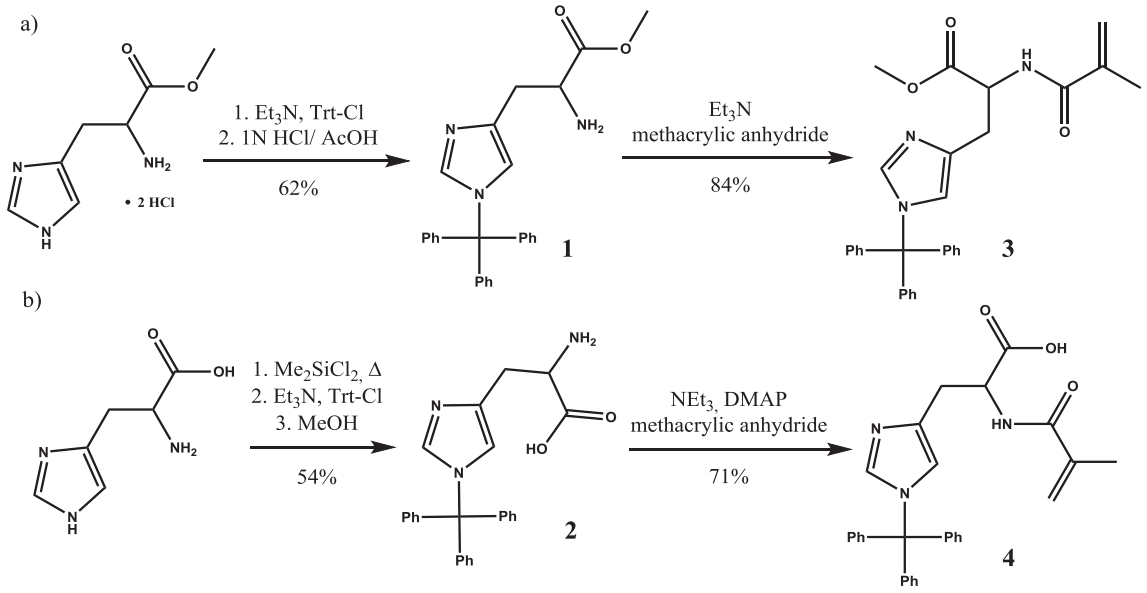

Scheme 1. Schematic representation of the synthetic pathway of a) N^{α}-methacryloyl-N^{τ}-tritylhistidine methyl ester (**3**) and b) N^{α}-methacryloyl-N^{τ}-tritylhistidine (**4**).

Table 4
Summary of the SEC results and thermal properties of the copolymers **P1** to **P8**.

Sample	$M_{n,SEC}$ [g/mol]	PDI	DSC: T_g [°C]	TGA: T_d [°C]	Histidine content [%][a]	Histidine content [%][b]
P1	15,500	1.08	45	288	9.1	7.1
P2	29,900	1.16	–	307	10	8.3
P3	14,800	1.17	50	312	10	10.2
P4	22,400	1.53	–	230	6.7	4.2
P5	18,000	1.08	38	346	9.1	6.7
P6	31,800	1.10	–	241	9.1	7.7
P7	16,600	1.16	47	302	9.1	8.8
P8	22,100	1.33	–	218	6.5	3.5

[a] Determined by ^{1}H NMR spectroscopy.
[b] Determined by elemental analyses.

Please cite this article in press as: Enke M, et al., Self-healing response in supramolecular polymers based on reversible zinc–histidine interactions, Polymer (2015), http://dx.doi.org/10.1016/j.polymer.2015.03.068

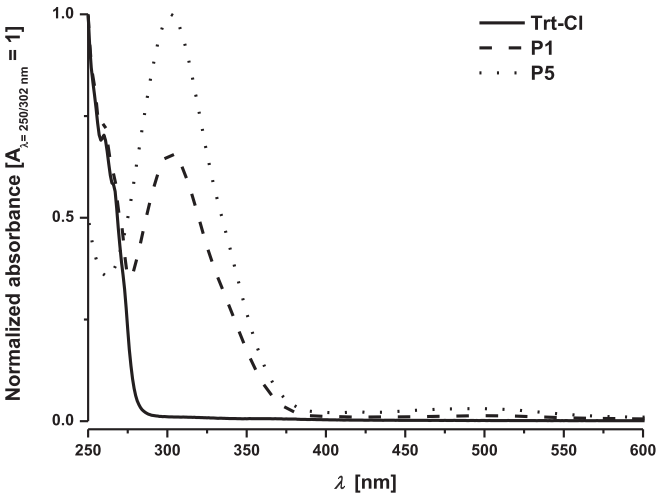

Fig. 1. UV-Vis spectrum of Trt-Cl, **P1** and **P5** ($CHCl_3$).

complex did not appear to result in the formation of ordered metallopolymer structures or alternatively, the metal-ligand exchange reaction is too fast.

The self-healing behavior was studied with the help of an optical microscope by cutting the copolymer films with a scalpel, resulting in scratches on the micrometer scale and, afterwards, heating to a defined temperature in an oven. Self-healing tests were repeated at the same place three times. An overview of the details of the self-healing behavior is provided in Table 5.

MP4 to **MP6** demonstrated the best self-healing tendency of the presented metallopolymers, perhaps due to the very flexible PLMA backbone. The materials were able to heal mechanical damage in the range of 40 – 60 °C, depending on the zinc salt used. More specifically, **MP4** revealed scratch healing at 50 °C, **MP5** at 60 °C and **MP6** at 40 °C, and notably, the scratches could be healed already within 20 min (Fig. 2). The first 5 min of the self-healing process is recorded and can be watched in the SI.

Furthermore, the mechanical properties of these copolymer networks were investigated by nanoindentation. The averaged indentation moduli were increasing from **MP4** to **MP6** and showed values from about 1.49 ± 0.04 GPa for **MP4**, 1.58 ± 0.05 GPa for **MP5** and 1.72 ± 0.14 GPa (rounded values, for details see Table S2). These values demonstrate a stiff polymeric material and indicate a crosslinked system, too [40–44]. From the load-depth curves, a typical behavior for elastoplastic material is visible [57], which is a requirement for the design of a self-healing material (Fig. S8, b–d). Furthermore, the material is getting softer from **MP6** to **MP4**, noticeable by overlaying the load-depth curves for maximum load (Fig. S8, e). Noticeably, the averaged hardness values of the metallopolymer networks **MP4** to **MP6** did not change, showing an average value of 56 ± 5 MPa (Table S2). Additionally, it was not possible to observe crack formation, phase transformation or delamination [58].

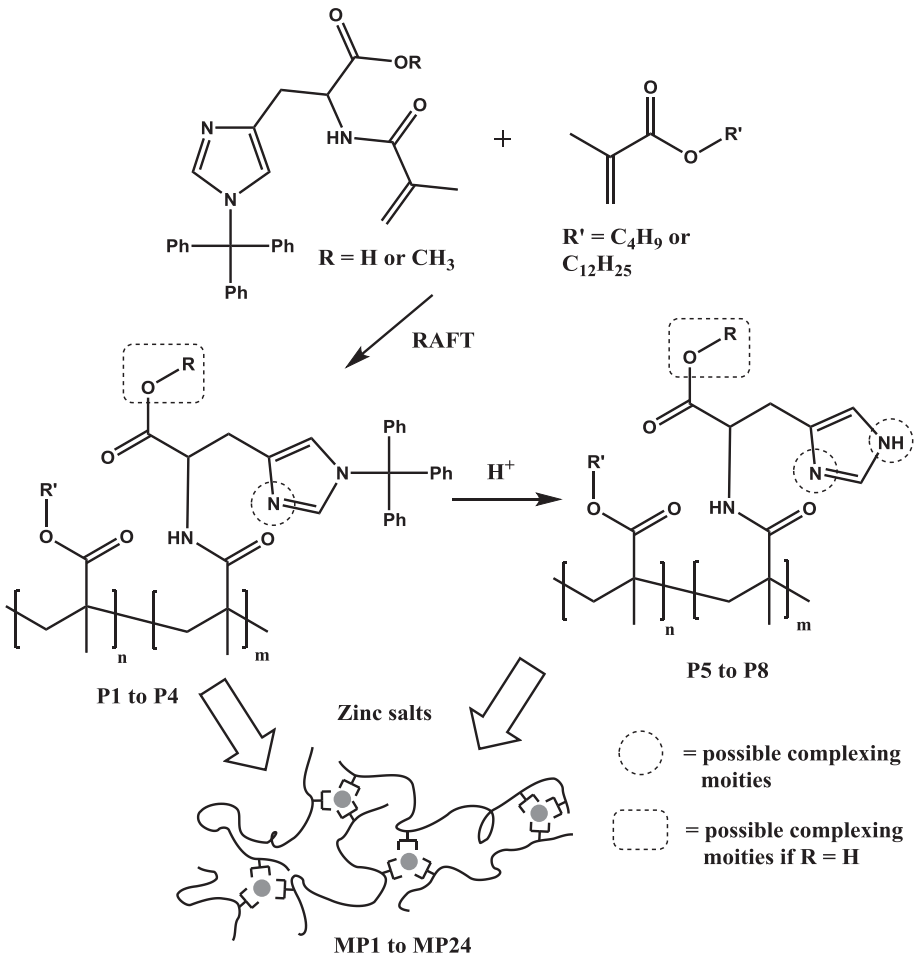

Scheme 2. Schematic representation of the synthesis and crosslinking of histidine containing copolymers with different zinc salts.

Please cite this article in press as: Enke M, et al., Self-healing response in supramolecular polymers based on reversible zinc–histidine interactions, Polymer (2015), http://dx.doi.org/10.1016/j.polymer.2015.03.068

Table 5
Results of the self-healing experiments of metallopolymers **MP1** to **MP24**.

Monomers	Metal salt	Metallopolymer	Self-healing ability temperature/time[c]	Metallopolymer	Self-healing ability temperature/time[c]
		With protecting group		Without protecting group	
3/BMA	$ZnCl_2$	**MP1**	No self-healing[a,b]	**MP13**	100 °C/20 h
3/BMA	$Zn(OAc)_2$	**MP2**	120 °C/20 h	**MP14**	150 °C/40 h
3/BMA	$Zn(NO_3)_2$	**MP3**	70 °C/38 h	**MP15**	100 °C/20h
3/LMA	$ZnCl_2$	**MP4**	50 °C/20 min	**MP16**	90 °C/18 h
3/LMA	$Zn(OAc)_2$	**MP5**	60 °C/20 min	**MP17**	100 °C/40 h
3/LMA	$Zn(NO_3)_2$	**MP6**	40 °C/20 min	**MP18**	No self-healing[b]
4/BMA	$ZnCl_2$	**MP7**	No self-healing[a,b]	**MP19**	No self-healing[a]
4/BMA	$Zn(OAc)_2$	**MP8**	No self-healing[a,b]	**MP20**	No self-healing[a]
4/BMA	$Zn(NO_3)_2$	**MP9**	No self-healing[a,b]	**MP21**	No self-healing[a]
4/LMA	$ZnCl_2$	**MP10**	100 °C/19 h	**MP22**	50 °C/19 h
4/LMA	$Zn(OAc)_2$	**MP11**	100 °C/20 h	**MP23**	50 °C/22 h
4/LMA	$Zn(NO_3)_2$	**MP12**	90 °C/60 h	**MP24**	RT/100 h

[a] Brittle films.
[b] No self-healing up to 150 °C.
[c] Lowest obtained temperatures and the resulting times.

The results outlined in Table 5 also indicate that the counter ions appear to have a significant influence on the ability and capacity to heal mechanical damage, as reported in literature for other systems [26]. Specifically, polymers crosslinked with zinc(II) acetate have the highest self-healing temperature and zinc(II) nitrate exhibited the lowest self-healing temperatures. This perhaps arises due to the strong binding between acetate and zinc. Weaker interactions between zinc and chloride, thus, may affect the self-healing temperature much less. In the case of nitrate, which is a non-coordinating counter ion, the best self-healing results were obtained. All metallopolymers containing histidine monomer **3** support this theory, except **MP1** (Fig. S9), which showed insufficient film formation and, thus, the self-healing properties could not be determined.

Furthermore, the cleavage of the protecting group leads to higher self-healing temperatures of **MP16** and **MP17**, if compared to **MP4** and **MP5**. One reason for that is the extended possibility to form crosslinks between histidine and zinc leading to higher binding strengths of the formed complexes compared with the interaction of zinc ions and Trt-protected histidine moieties. Therefore, the cleavage of the crosslinks to enable flexibility of the polymer chains requires more energy and, thus, an increased temperature. Additionally, the counter ions do not affect the self-

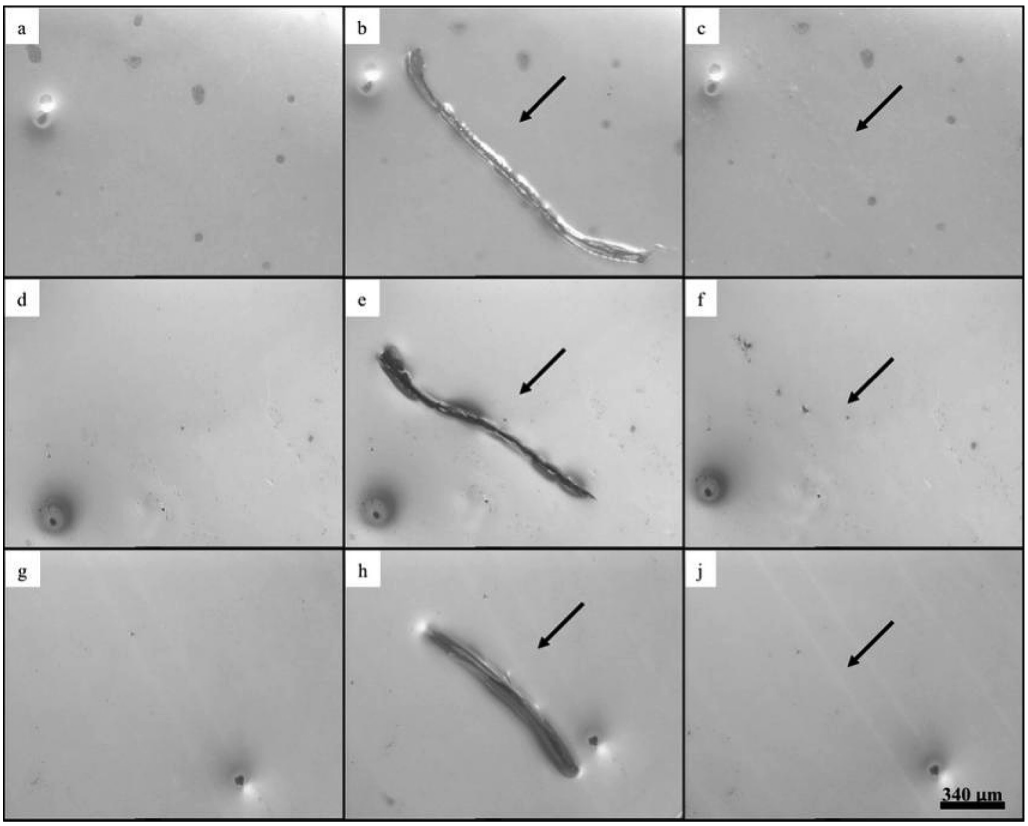

Fig. 2. Self-healing experiments of **MP4** to **MP6**. (a) Film without scratch (**MP4**), (b) scratch, (c) healing after 20 min at 50 °C, (d) film without scratch (**MP5**), (e) scratch, (f) healing after 20 min at 60 °C, (g) film without scratch (**MP6**), (h) scratch and (j) healing after 20 min at 40 °C.

Please cite this article in press as: Enke M, et al., Self-healing response in supramolecular polymers based on reversible zinc–histidine interactions, Polymer (2015), http://dx.doi.org/10.1016/j.polymer.2015.03.068

healing temperature to such an extent, which could also be explained by the stronger zinc–histidine interactions. **MP15**, crosslinked with zinc (II) nitrate, shows no improvement of the self-healing properties compared with **MP13** (crosslinked with zinc (II) chloride). Thus, the influence of the counter ion interaction appears to be different when compared to systems featuring a protecting group. In addition, **MP18** demonstrated no self-healing behavior in contrast to **MP16**. A possible explanation for the obtained differences could be the formation of an additional new superstructure within the resulting materials; however, this remains to be determined.

In the case of metallopolymers containing histidine monomer **4**, the free carboxylic acid influences the self-healing properties in a different way, as described above. In general, the presence of the carboxylic acid functionality decreases the flexibility of the resulting networks, possibly due to formation of new supramolecular crosslinks. As a consequence, metallopolymers with BMA as co-monomer formed highly brittle films (Fig. S10). However, changing the co-monomer to LMA improved the film forming properties and self-healing investigations could be carried out (**MP10** to **MP12)** (Fig. S11 and Fig. S12). In particular, for those systems another property of the films could be observed – namely that the required self-healing time was found to strongly depend on the size of the scratch. Films of **MP10** were firstly treated with a relatively broad scratch, which takes 80 h to heal at 100 °C. The second scratch was thin and could be healed within 19 h at the same temperature. Furthermore, the material contact in the case of the second scratch also improves the self-healing behavior, possibly leading to a kind of a "zipping effect" [59].

After the cleavage of the protecting group, the self-healing behavior of **MP22** to **MP24** (Fig. S14) improved significantly, which is completely different to self-healing behavior of the metallopolymers containing **3**. In contrast to our study, there are several studies investigating unsubstituted histidine systems. In these cases, the Im-*N* and the free amino base are usually coordinating the metal ions [60,61]. In fact, zinc typically coordinates four to six ligands [61]. X-ray absorption spectroscopy (XAS) of $Zn(His)_2$ in neutral solution indicates a tetrahedral geometry and in a slightly acidified medium (pH ~ 5.9) the geometry is changing to an octahedral geometry with monodentate histidine ligands [62]. In contrast, the histidine moieties presented here are substituted. Thus, the coordination properties of the better characterized imidazole ring can be utilized to give a general overview as well as a guideline for understanding the here presented materials without speculations [63]. The investigation of methyl-substituted imidazole rings either on position 1 or 4 (complexed with $ZnCl_2$) by NMR relaxometry pointed out that the stability constant of the Me(4)-Im is lower compared to Me(1)-Im [64]. The imidazole ring of histidine is always substituted at position Im-4. In case of the materials containing histidine monomer **3**, the sterically demanding trityl-group protects position Im-1, as well as the methylester blocks the carboxylic acid and the polymerizable group attached on the amino function. Therefore a weak zinc–histidine interaction seems likely, which correlates well with the relatively low self-healing temperatures of these metallopolymers.

Materials containing **4** feature a carboxylic acid moiety, which can also coordinate with zinc ions. NMR studies of zinc-binding histidine-containing proteins demonstrated that zinc(II) ions will easily form a pentahedral coordination with three histidines and two carboxyl units [61]. These results may suggest an equal coordination structure of the crosslinks at **MP22** to **MP24**. The sterically demanding trityl-group by **MP10** to **MP12**, on the other hand, could prevent this preferred coordination structure or could lead to disordered conformations, increasing the self-healing temperature significantly. Thus, free carboxylic acid moieties appear to have a large impact on the self-healing properties due to changed coordination behavior.

4. Conclusions and outlook

In this study, histidine-rich polymer networks inspired by reversible crosslinks observed in mussel byssal threads were produced, and the self-healing properties were investigated in the presence of different zinc salts. For this purpose, two new histidine monomers (**3**/**4**) were synthesized and subsequently copolymerized with butyl methacrylate (BMA) and lauryl methacrylate (LMA) (**P1** to **P4**) utilizing the RAFT polymerization technique. Afterwards, the Trt-group was cleaved off to mimic the mussel system (**P5** to **P8**), and the crosslinking of protected and unprotected histidine containing copolymers was performed with several zinc salts (zinc(II) chloride, zinc(II) acetate and zinc(II) nitrate), leading to metallopolymers with temperature-dependent self-healing behavior (**MP1** to **MP24**). The findings indicate that metallopolymers with LMA exhibited the best self-healing behavior. The longer side chains and the lower glass transition temperature (T_g) of PLMA may provide the required flexibility of the material which is necessary to facilitate the self-healing process. Furthermore, the influence of the counter ion on the self-healing temperature was investigated. In general, a stronger interaction of the metal ion with the counter ion leads to higher self-healing temperatures. Thus, the complexing acetate counter ion, which features the strongest interaction with zinc, has the worst self-healing behavior. For instance, **MP5** (crosslinked with Zn(II) acetate) requires 60 °C to heal in 20 min whereas **MP6** (crosslinked with Zn(II) nitrate) recovers at 40 °C in the same time frame. However, the unprotected histidine containing metallopolymers (**MP13** to **MP24**) showed a tendency to higher self-healing temperatures and only a minor influence of the counter ion. The removal of the protection group may enable an extended possibility to build up crosslinks, which results in a higher binding strength of the zinc–histidine interactions and, thus, more energy is required to cleave those reversible crosslinks and the counter ion effect is less prominent. To summarize, we have synthesized histidine-rich self-healing materials based on coordination chemistry found in mussel byssal threads that exhibit zinc salt dependent healing temperatures.

In the future, a deeper understanding of the molecular interactions will be investigated in order to get a better comparison between the natural and the synthetic self-healing metallopolymers. For this purpose, other histidine monomers as well as other metal salts will be utilized. Furthermore, the coordination structure of metal-histidine crosslinks will be investigated in detail in order to optimize these interactions and to selectively tune the self-healing behavior of such materials.

Acknowledgments

The authors thank the Deutsche Forschungsgemeinschaft (DFG, SPP 1568) and the Fonds der chemischen Industrie (FCI) (scholarship for S.B.) for financial support. M.J.H. acknowledges the Max Planck Society for financial support. F. H. S. and U. S. S. are further grateful to the Thuringian Ministry for education, Science, and Culture (TMBWK, #B515-11028, SWAXS-JCSM) for financial support.

Appendix A. Supplementary data

Supplementary data related to this article can be found at http://dx.doi.org/10.1016/j.polymer.2015.03.068.

References

[1] Dry CM, Sottos NR. In: North American conference on smart structures materials; 1993. p. 438–44. Albuquerque.
[2] White SR, Sottos NR, Geubelle PH, Moore JS, Kessler MR, Sriram SR, et al. Nature 2001;409:794–7.
[3] Garcia SJ. Eur Polym J 2014;53:118–25.
[4] Zedler L, Hager MD, Schubert US, Harrington MJ, Schmitt M, Popp J, et al. Mater Today 2014;17:57–69.
[5] Degtyar E, Harrington MJ, Politi Y, Fratzl P. Angew Chem Int Ed 2014;53:12026–44.
[6] Hager MD, Greil P, Leyens C, van der Zwaag S, Schubert US. Adv Mater 2010;22:5424–30.
[7] Herbst F, Döhler D, Michael P, Binder WH. Macromol Rapid Commun 2013;34:203–20.
[8] Chen X, Dam MA, Ono K, Mal A, Shen H, Nutt SR, et al. Sciene 2002;295:1698–702.
[9] Chen X, Wudl F, Mal AK, Shen H, Nutt SR. Macromolecules 2003;36:1802–7.
[10] Kötteritzsch J, Stumpf S, Hoeppener S, Vitz J, Hager MD, Schubert US. Macromol Chem Phys 2013;214:1636–49.
[11] Oehlenschlaeger KK, Mueller JO, Brandt J, Hilf S, Lederer A, Wilhelm M, et al. Adv Mater 2014;26:3561–6.
[12] AbdolahZadeh M, Esteves ACC, van der Zwaag S, Garcia SJ. J Polym Sci Part A: Polym Chem 2014;52:1953–61.
[13] Amamoto Y, Kamada J, Otsuka H, Takahara A, Matyjaszewski K. Angew Chem Int Ed 2011;50:1660–3.
[14] Lafont U, van Zeijl H, van der Zwaag S. ACS Appl Mater Interfaces 2012;4:6280–8.
[15] Cordier P, Tournilhac F, Soulié-Ziakovic C, Leibler L. Nature 2008;451:977–80.
[16] Montarnal D, Cordier P, Soulié-Ziakovic C, Tournilhac F, Leibler L. J Polym Sci Part A: Polym Chem 2008;46:7925–36.
[17] Herbst F, Seiffert S, Binder WH. Polym Chem 2012;3:3084–92.
[18] Chen Y, Kushner AM, Williams GA, Guan Z. Nat Chem 2012;4:467–72.
[19] Burattini S, Colquhoun HM, Fox JD, Friedmann D, Greenland BW, Harris PJF, et al. Chem Commun 2009:6717–9.
[20] Burattini S, Colquhoun HM, Greenland BW, Hayes W. Faraday Discuss 2009;143:251–75.
[21] Burattini S, Greenland BW, Merino DH, Weng W, Seppala J, Colquhoun HM, et al. J Am Chem Soc 2010;132:12051–8.
[22] Hart LR, Hunter JH, Nguyen NA, Harries JL, Greenland BW, Mackay ME, et al. Polym Chem 2014;5:3680–8.
[23] Vega JM, Grande AM, van der Zwaag S, Garcia SJ. Eur Polym J 2014;57:121–6.
[24] Kalista SJ, Pflug JR, Varley RJ. Polym Chem 2013;4:4910–26.
[25] Bode S, Zedler L, Schacher FH, Dietzek B, Schmitt M, Popp J, et al. Adv Mater 2013;25:1634–8.
[26] Bode S, Bose RK, Matthes S, Ehrhardt M, Seifert A, Schacher FH, et al. Polym Chem 2013;4:4966–73.
[27] Burnworth M, Tang L, Kumpfer JR, Duncan AJ, Beyer FL, Fiore GL, et al. Nature 2011;472:334–7.
[28] Kupfer S, Zedler L, Guthmuller J, Bode S, Hager MD, Schubert US, et al. Phys Chem Chem Phys 2014;16:12422–32.
[29] Sandmann B, Bode S, Hager MD, Schubert US. Adv Polym Sci 2013;262:239–58.
[30] Mozhdehi D, Ayala S, Cromwell OR, Guan Z. J Amer Chem Soc 2014;136:16128–31.
[31] Holten-Andersen N, Harrington MJ, Birkedal H, Lee BP, Messersmith PB, Lee KYC, et al. Proc Natl Acad Sci U. S. A 2011;108:2651–5.
[32] Harrington MJ, Masic A, Holten-Andersen N, Waite JH, Fratzl P. Sciene 2010;328:216–20.
[33] Vaccaro E, Waite JH. Biomacromolecules 2001;2:906–11.
[34] Harrington MJ, Waite JH. J Exp Biol 2007;210:4307–18.
[35] Carrington E, Gosline JM. Am Malacol Bull 2004;18:135–42.
[36] Harrington MJ, Gupta HS, Fratzl P, Waite JH. J Struc Biol 2009;167:47–54.
[37] Schmidt S, Reinecke A, Wojcik F, Pussak D, Hartmann L, Harrington MJ. Biomacromolecules 2014;15:1644–52.
[38] Fullenkamp DE, He L, Barrett DG, Burghardt WR, Messersmith PB. Macromolecules 2013;46:1167–74.
[39] Srivastava A, Holten-Andersen N, Stucky GD, Waite JH. Biomacromolecules 2008;9:2873–80.
[40] Rettler EFJ, Kranenburg JM, Lambermont-Thijs HML, Hoogenboom R, Schubert US. Macromol Chem Phys 2010;211:2443–8.
[41] Oyen ML, Cook RF. J Mater Res 2003;18:139–50.
[42] Oyen ML, Cook RF. J Mech Behav Biomed Mater 2009;2:396–407.
[43] Oliver WC, Pharr GM. J Mater Res 1992;7:1564–83.
[44] Oliver WC, Pharr GM. J Mater Res 2004;19:3–20.
[45] Himes RA, Park GY, Siluvai GS, Blackburn NJ, Karlin KD. Angew Chem Int Ed 2008;47:9084–7.
[46] Barlos K, Papaioannou D, Theodoropoulos D. J Org Chem 1982;47:1324–6.
[47] Sagert J, Waite JH. J Exp Biol 2009;212:2224–36.
[48] Dudev T, Lin, Dudev M, Lim C. J Am Chem Soc 2003;125:3168–80.
[49] Moad G, Rizzardo E, Thang SH. Aust J Chem 2005;58:379–410.
[50] Chiefari J, Chong YK, Ercole F, Krstina J, Jeffery J, Le TPT, et al. Macromolecules 1998;31:5559–62.
[51] Moad G, Rizzardo E, Thang SH. Aust J Chem 2009;62:1402–72.
[52] Agelis G, Resvani A, Koukoulitsa C, Tumova T, Slaninova J, Kalavrizioti D, et al. Eur J Med Chem 2013;62:352–70.
[53] Bode S, Enke M, Görls H, Hoeppener S, Weberskirch R, Hager MD, et al. Polym Chem 2014;5:2574–82.
[54] Xu Y, Becker H, Yuan J, Burkhardt M, Zhang Y, Walther A, et al. Macromol Chem Phys 2007;208:1666–75.
[55] Lichtenegger HC, Schoberl T, Ruokolainen JT, Cross JO, Heald SM, Birkedal H, et al. Proc Natl Acad Sci U. S. A 2003;100:9144–9.
[56] Fleischhaker F, Haehnel AP, Misske AM, Blanchot M, Haremza S, Barner-Kowollik C. Macromol Chem Phys 2014;215:1192–200.
[57] Fischer-Cripps AC. Nanoindentation, 1. Springer; 2011.
[58] Menčík J. Uncertainties and errors in nanoindentation. 2012.
[59] Kalista SJ. Self-healing ionomers. In: Ghosh SK, editor. Self-healing materials: fundamentals, design strategies and applications. Weinheim: Wiley-VCH; 2009. p. 91.
[60] Förster M, Vahrenkamp H. Chem Ber 1995;128:541–50.
[61] Zoroddu MA, Medici S, Peana M, Anedda R. Dalton Trans 2010;39:1282–94.
[62] Ferrer P, Jiménez-Villacorta F, Rubio-Zuazo J, da Silva I, Castro GR. J Phys Chem B 2014;118:2842–50.
[63] Andersson Trojer M, Movahedi A, Blanck H, Nydén M. J Chem 2013;2013:23.
[64] Andersson M, Hedin J, Johansson P, Nordström J, Nydén M. J Phys Chem A 2010;114:13146–53.

Please cite this article in press as: Enke M, et al., Self-healing response in supramolecular polymers based on reversible zinc–histidine interactions, Polymer (2015), http://dx.doi.org/10.1016/j.polymer.2015.03.068